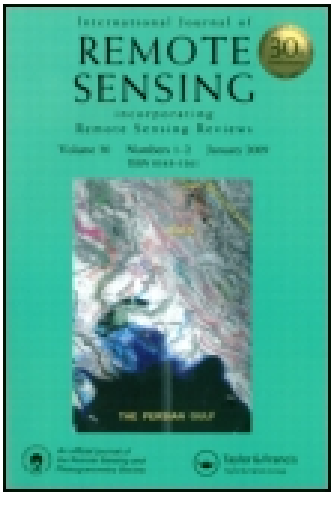

International Journal of Remote Sensing
Publication details, including instructions for authors and subscription information:
http://www.tandfonline.com/loi/tres20

Land-use and land-cover classification in semi-arid regions using independent component analysis (ICA) and expert classification

Mohammad Namdar[a], Jan Adamowski[b], Hossein Saadat[b], Forood Sharifi[c] & Afsaneh Khiri[a]

[a] Forest, Range and Watershed Management Organization, Lashgark Road, Tehran, Iran

[b] Department of Bioresource Engineering, McGill University, Ste-Anne-de-Bellevue, Quebec, Canada H9X 3V9

[c] Soil Conservation and Watershed Management Research Institute, P.O. Box 13445, Tehran, Iran

Published online: 04 Dec 2014.

To cite this article: Mohammad Namdar, Jan Adamowski, Hossein Saadat, Forood Sharifi & Afsaneh Khiri (2014) Land-use and land-cover classification in semi-arid regions using independent component analysis (ICA) and expert classification, International Journal of Remote Sensing, 35:24, 8057-8073, DOI: 10.1080/01431161.2014.978035

To link to this article: http://dx.doi.org/10.1080/01431161.2014.978035

International Journal of Remote Sensing, 2014
Vol. 35, No. 24, 8057–8073, http://dx.doi.org/10.1080/01431161.2014.978035

Land-use and land-cover classification in semi-arid regions using independent component analysis (ICA) and expert classification

Mohammad Namdar[a], Jan Adamowski[b]*, Hossein Saadat[b], Forood Sharifi[c], and Afsaneh Khiri[a]

[a]*Forest, Range and Watershed Management Organization, Lashgark Road, Tehran, Iran;* [b]*Department of Bioresource Engineering, McGill University, Ste-Anne-de-Bellevue, Quebec, Canada H9X 3V9;* [c]*Soil Conservation and Watershed Management Research Institute, P.O. Box 13445, Tehran, Iran*

(*Received 16 October 2013; accepted 10 September 2014*)

This study was focused on addressing the need for accurate land-use/land-cover classification (LULC) maps in Iran and in other similarly developing countries. To generate and validate a new LULC map for northeastern Iran's 2037.5 km^2 Hable-roud watershed, a step-by-step process was developed and implemented, consisting of image preprocessing, extraction of training and reference sampling locations, decomposition of multi-spectral thematic mapper bands into features by independent component analysis methods, classification using these features and slope maps, enhancement of land-use classes through image segmentation and zonal statistics, then through consideration of normalized difference vegetation index and climatic zones, followed by ground truthing. This newly developed approach provided maps that distinguished dryland farming, irrigated farmland, forest plantations, and low-, medium-, and high-vegetation density rangelands, while currently available maps for the watershed left 39% of lands unclassified or in combined classes. The new maps' ground-truthing-based overall accuracy and kappa coefficient were 88.3% and 0.83, respectively. In order to develop such an improved LULC map, it was necessary to go beyond the mere analysis of reflectance information, to incorporating climatic and topographic data through this newly proposed step-by-step approach.

1. Introduction

With a mean annual rainfall of 240 mm, and roughly 90% of its territory classed as arid or semi-arid, Iran is a dry land area. Of the nation's 1.65×10^6 km^2 total area, about 0.37×10^6 km^2 are arable and of this 54% is irrigated and the remainder devoted to dryland farming (Mousavi 2005). Most Iranian farms are small, with only 22% exceeding 10 ha in area and 11% being less than 1 ha in extent (Mousavi 2005). Areas in their natural state or existing as rangeland total 1.024×10^6 km^2, of which pastures (at various levels of forage productivity) and forests contribute 88% and 12%, respectively. In many of Iran's arid and semi-arid regions, and in particular in the Hable-Roud watershed that is the focus of this study, significant overgrazing and inappropriate land use (e.g. steep hillside farming, up–downslope tillage) are the main contributors to soil erosion and land degradation. Accurate land-use/land-cover classification (LULC) maps can be very useful tools in watershed management, and in particular in soil erosion control efforts and decision-making with respect to which lands are capable of sustaining agriculture and which are not (Cihlar 2000; Renschler and Harbor 2002).

*Corresponding author. Email: jan.adamowski@mcgill.ca

Poor soil and lack of adequate water distribution has led agriculturalists to resort to dryland farming. Dryland farming systems are very diverse, including a variety of shifting agriculture systems, annual croplands, home gardens, mixed agriculture–livestock systems, as well as nomadic pastoral and transhumance systems. The soil is generally too dry to adequately plough after harvest. If a field remains uncultivated, weeds may grow (Koohafkan and Stewart 2008). This results in the inaccurate classification of land use and land cover from the analysis of remote-sensing data given the spectral mixture and spatial heterogeneity.

Using aerial photographs and topographic maps, the Iranian Forest, Range and Watershed Management Organization has been involved in mapping LULC for the last 50 years. Recently, satellite imagery have been employed in LULC classification; however, this raises certain issues related to existing LULC maps: (i) polygon boundaries of main land uses (i.e. irrigated farming, dryland farming, rangeland and forest classes) have been found to be inaccurate and show significant overlap; (ii) separation into classes of irrigated vs. dryland farming is generally not possible; and (iii) roughly 15% of the land area was classed as 'mixed', with separation into individual classes not being possible (Saadat and Namdar 2012). In light of these issues, the goal of the present study was to develop a new protocol for LULC classification using a large semi-arid study area (2037.5 km^2) based on readily available ancillary information, independent component analysis (ICA), and expert classification. This research methodology has been devised using a multidisciplinary and hierarchical approach.

LULC classification is one of the most common applications of remote-sensing data. Any given remote-sensing image can be decomposed into several objects exhibiting similar spectral characteristics. Therefore, the main objective of a feature extraction technique is to accurately retrieve these features. There are a large number of standardized classification schemes used for land-use and land-cover maps throughout the world. The most commonly used approaches include unsupervised classification, supervised classification, vegetation indices, object-based image analysis (OBIC), and support vector machines, among others. Each of these methods has its own restrictions and advantages, but none can individually create an acceptable level of accuracy in producing LULC maps in most cases.

Spectral enhancement methods can be useful in ensuring accurate image classification. ICA is a mathematical tool for extracting factors or components that underlie sets of random variables, measurements, or signals (Du, Kopriva, and Szu 2006; Naik and Kumar 2011). Chen et al. (2008), using ICA to improve image classification accuracy, found it not only to be effective in removing correlation amongst multi-spectral images, but also in allowing sparse coding of images and capturing the essential edge structures and textures of images. Experimental results demonstrating that the ICA algorithm can effectively improve the accuracy of image classification highlight the ability of ICA to perform unsupervised classification (Du, Kopriva, and Szu 2006).

Ozdogan (2010) reported on the usefulness of the ICA signal processing algorithm's ability to temporally decompose Moderate Resolution Imaging Spectroradiometer (MODIS) data to automatically map major crop types in three agricultural regions (Kansas and Nebraska in the USA, and northwestern Turkey). Based on the premise that when cultivated fields were smaller than the spatial resolution of a moderate-resolution sensor, then temporal profiles of individual crops in the resulting images were observed as mixtures. Chitroub and AlSultan (2008), employing ICA for seasonal analysis of vegetation, found that the extracted independent component (IC) images were particularly informative regarding the surface state of the observed scene. This was especially the

case with respect to the stability and transition zones of the vegetation, compared with the extracted PC images.

The development of segmentation-based image analysis (often named object-based image analysis, OBIA) applications has blossomed in the last 10 years (Woodcock and Harward 1992; Lobo 1997; Blaschke, Burnett, and Pekkarinen 2004; Blaschke, Lang, and Hay 2008; Im, Jensen, and Tullis 2008; Gamanya, de Maeyer, and de Dapper 2009). Other researchers have similarly concluded that overall accuracy is significantly higher when using OBIA *versus* traditional methods (Chen et al. 2007; Lackner and Conway 2008; Blaschke 2010).

Using a number of ancillary layers (e.g. landform and climatic zone maps) to assist in the interpretation and classification of remotely sensed imagery for LULC mapping, Saadat et al. (2011) showed that successful mapping depends on more than just analysis of reflectance information: incorporating climatic and topographic conditions helped delineate what was otherwise overlapping information.

It is well known that a significant correlation exists between spectral data and different vegetation growth parameters (Thenkabail et al. 2004; Tian et al. 2007; Houborg and Boegh 2008; Saadat et al. 2011). Guerschman et al. (2003) recommended that, when possible, three images (spring, early summer, late summer) be used to identify summer crops, winter crops, and rangelands. Saadat et al. (2011) demonstrated that, in the case of funding constraints to obtaining more than one image, late-summer images were more suitable for LULC mapping.

Shaped through a multidisciplinary and hierarchical approach, the present study's principal objective and novelty is to propose a new protocol for LULC classification in semi-arid regions using late-summer Landsat TM images. This classification relies on readily available ancillary information, ICA, and expert classification.

2. Methods and materials

2.1. Study area

Iran's Hable-Roud watershed, located between 52° 16′ and 53° 08′ E longitude and 35° 27′ and 35° 57′ N latitude, covers an area of 2037.5 km^2 in the northeastern portion of Tehran Province (Figure 1). Composed of a complex combination of mountains, hills, plains, and rivers, the watershed ranges from 1443 to 4051 m in elevation above mean sea level (AMSE). Given its geographic location and topography, a wide range of climates prevails across the different portions of the Hable-Roud watershed (i.e. semi-arid cold to dry). Mean annual precipitation is 318 mm and mean annual air temperature is 8.7°C. March is the month of highest rainfall, at 79 mm on average (Royan Consulting Engineering 2008). Existing landform maps show 69.13% of the Hable-Roud watershed to be mountainous, with the remaining landforms being: 153.6 ha (0.07% of total area) river alluvial plains, 2271.8 ha (1.01%) piedmont plains, 1701.6 ha (0.75%) alluvial fans, 31,552.8 ha (13.98%) upper terraces, 3701.2 ha (1.64%) river terraces, and 30,282.5 ha (13.42%) hills (Saadat and Namdar 2012).

2.2. Land-use and land-cover classification

To classify land use and land cover from a late-summer Landsat TM5 image (7 August 2010, scene 164–35, US Geological Survey), six steps (Figure 2) were undertaken: (i) image preprocessing; (ii) random extraction of training and reference sampling locations;

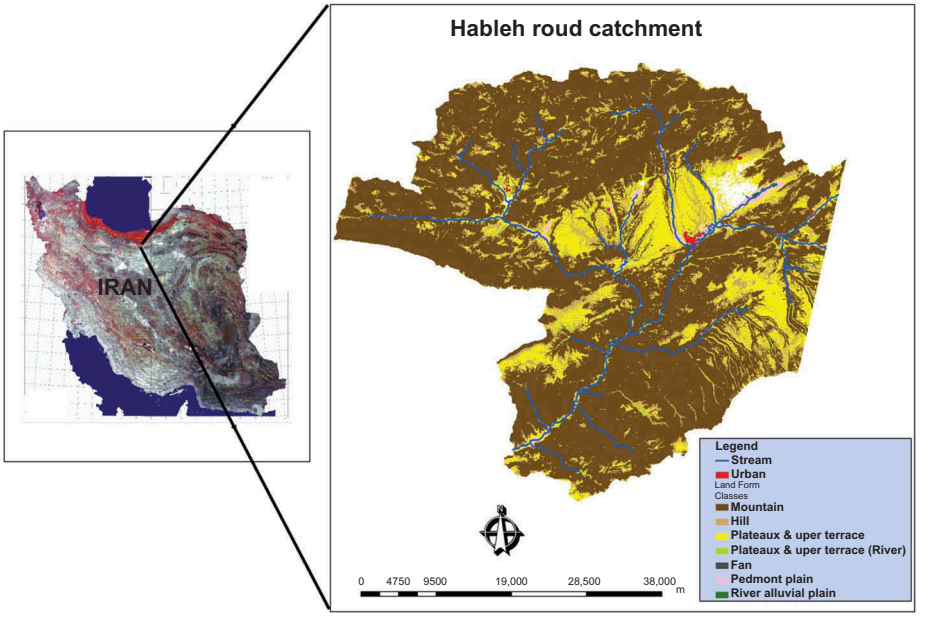

Figure 1. Location of the study area.

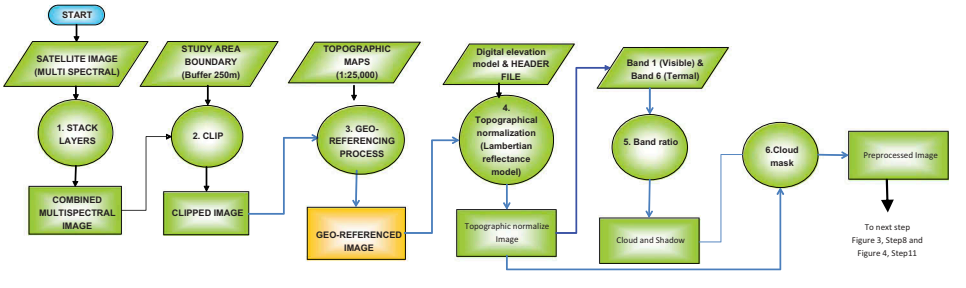

Figure 2. Image preprocessing.

(iii) decomposition of multi-spectral TM bands into features using the ICA method; (iv) expert classification using the slope map and features extracted by the ICA method; (v) enhancement of the classified land-use map via image segmentation and zonal statistics; and (vi) enhancement of the classified land-cover map via the normalized difference vegetation index (NDVI) and climatic zones. By combining the outputs of the last two steps, a final LULC map was created. Upon completion of all these steps the accuracy of the final LULC map was evaluated. ERDAS IMAGINE (Version 9.2) was used for all image geo-processing and ArcMap (Version 9.3) software was used for the GPS data.

2.2.1. *Image preprocessing*

Landsat TM images have seven individual bands, each representing a single layer of continuous imagery. Given their low spatial resolution (60 m), the thermal band was used

solely for cloud removal. The image's non-thermal bands (30 m) were combined into a multi-layer image and clipped with a 250 m exterior buffer around the study area boundary (Figure 2. steps 1 and 2). The satellite data were geometrically registered using a second-order polynomial transformation. Uniformly distributed ground control points (GCPs) were employed such that the root mean square error was less than 0.33 pixel.

Since almost 70% of the study area is mountainous, topographical normalization was employed to remove the potential effects of differential illumination and shadowing caused by terrain variability on spectral reflectance. This involved using Lambertian reflectance models to transform data in such a manner as to normalize the imagery, rendering it as if it were a flat surface (Smith, Lin, and And Ranson 1980; Colby 1991). This transformation required the solar elevation and azimuth at time of image acquisition (header file), a digital elevation model (DEM) based on 1:25,000 digital topographic maps (obtained from the National Cartographic Centre of Iran), and the original imagery file (TM). The coordinate system used in the topographic maps was Universal Transverse Mercator (UTM) zone 39 with spheroid and datum WGS84.

Around 0.5% of the image was covered by clouds. As clouds were reflective (high) in Band 1 and cold (low) in Band 6, the ratio of the two bands was high over clouds (Martinuzzi, Gould, and Ramos González 2007). Therefore, a new image, where cloudy parts were masked out from the original image, was produced by thresholding on this ratio. Since the cloudy area in the image was very small, a fill process was not performed.

2.2.2. *Stratified design of training and reference sampling sites*

Training and reference sampling locations were chosen by stratified random sampling to include a full variety of potential LULC classes across the entire study area. Since this study encompassed a relatively large watershed, with different climatic zones and a complex terrain, we first combined three ancillary layers to generate a map with 24 initial strata (Figure 3, step 7).

- a 1:25,000 scale landform map prepared by Saadat et al. (2008);
- a 1:25,000 scale classified slope map prepared by Saadat and Namdar (2012); and
- a 1:50,000 scale climatic zone map prepared by Royan Consulting Engineers (2008),

We further combined this initial stratification map with an unsupervised classification image of the Landsat TM (ISODATA method, with a maximum of 12 iterations and a 95% convergence threshold) with 18 classes (Figure 3, steps 8 and 9). The resulting base map for the stratification featured 145 strata. Using a stratified random sampling procedure (Stehman 1999), 410 training and 410 reference sampling locations were distributed across the base map (Figure 3, step 10). Of the 820 training/reference sampling locations, 14 were essentially inaccessible due to physical barriers or their remoteness from roads. These sites were replaced by 14 accessible sites within the same classes. Because urban areas represented less than 1% of the total area and were easily recognizable on the image, these regions were ignored on field visits.

2.2.3. *Decomposition of multi-spectral TM bands into features using the ICA method*

ICA performs a linear transformation of the spectral bands such that the resulting components are decorrelated and independent (Figure 4, Step 11). Each IC contains

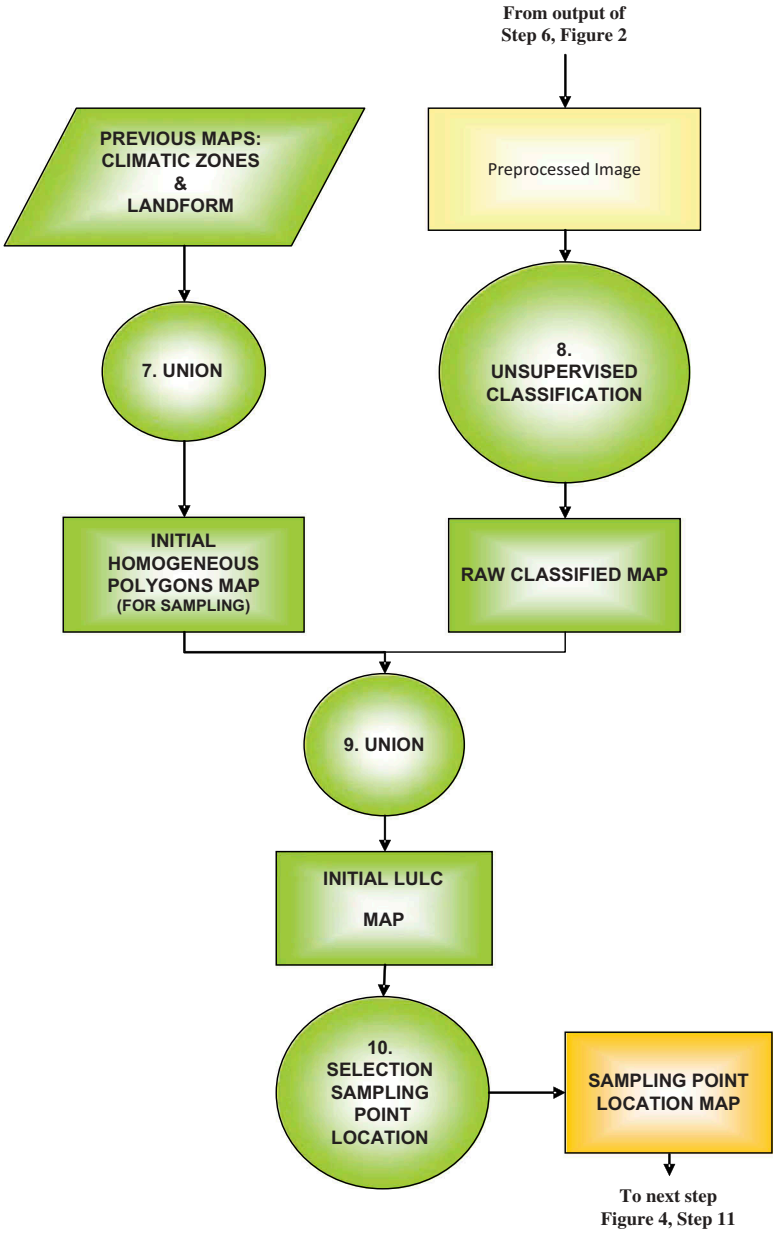

Figure 3. Extraction of a training and reference sampling location map.

information corresponding to a specific feature in the original image. Detailed descriptions of the mathematical formulation of ICA are given in Shah (2003) and Comon (1994). ICA exploits the higher-order statistical characteristics of multi-spectral and hyperspectral imagery (e.g. skewness and kurtosis). Skewness and kurtosis are, respectively, measures of asymmetry and peakedness/flatness on an image histogram. Based on histograms derived from different bands, a combination of three measurements was used for

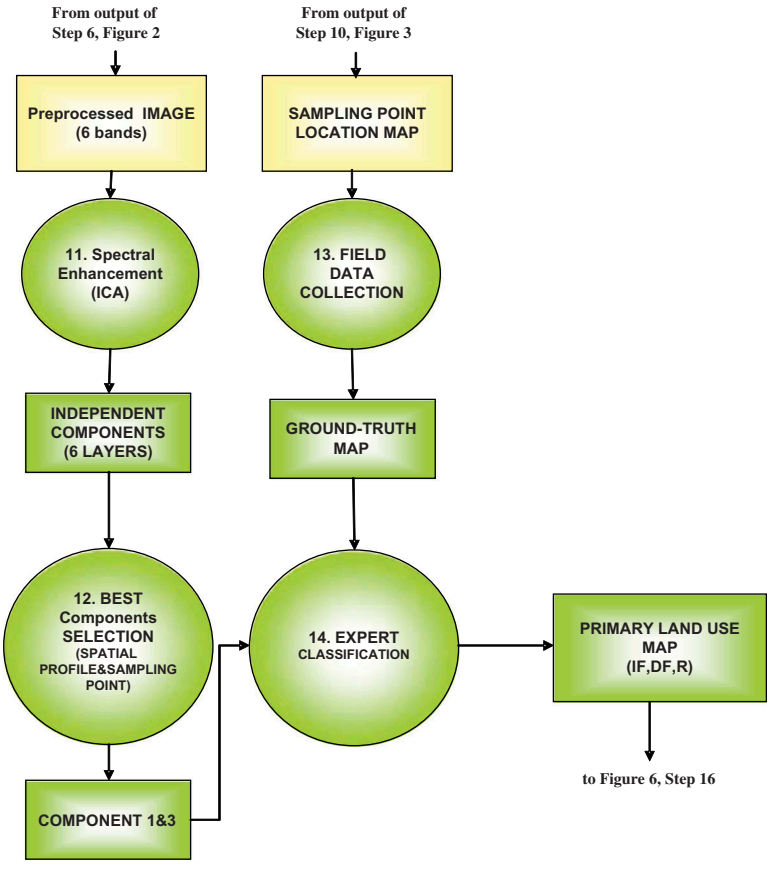

Figure 4. Decomposition of multi-spectral TM bands into features using the ICA method and subsequent expert classification using ICA features and slope map.

component ordering: correlation × skewness × kurtosis. From six TM bands, six ICs were extracted (Figure 4, Step 12), and these were scrutinized for their ability to distinguish irrigated farming from dryland farming. ICA Component 1 was distinctive for irrigated farming, while ICA Component 3 was distinctive for dryland farming (Figure 5).

2.2.4. *Expert classification using ICA features and slope map*

Using an expert classification strategy with non-parametric, variable range-based rules, coupled with an elimination process, we defined a hierarchical decision tree based on ICA1, ICA3, and slope (Table 1), resulting in four possible outcomes for agriculture activities: Dryland Farming (DF), Irrigated Farming (IR), Man-Made Forest (FMM), and Rangeland (R).

2.2.5. *Image segmentation and zonal statistics*

An image segmentation algorithm was applied to the six bands of the Landsat TM image (Figure 6, Step 15) using the Bonnie Ruefenacht algorithm (Ruefenacht et al. 2002). The

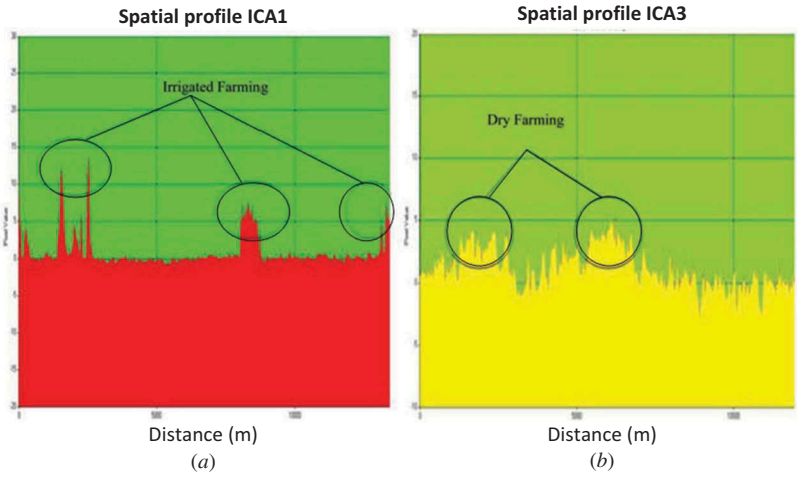

Figure 5. Spatial profile of (*a*) ICA Component 1, distinctive for irrigated farming, and (*b*) ICA Component 3, distinctive for dryland farming.

Table 1. Classification criteria for Irrigated Farming, Dryland Farming, Man-Made Forest, and Rangeland.

Class	Data for classification	Rules
Irrigated Farming (IR)	ICA_1, slope	$29.516 > ICA_1 \geq 3.0$ and Slope $\leq 5\%$
Dryland Farming (DF)	ICA_3, slope	$ICA_3 \geq 3.0$ and $ICA_1 < 3.9$ and Slope $\leq 20\%$
Man-Made Forest (FMM)	ICA_1, slope	$0.4 > ICA_1 \geq 0.1$ and $15\% >$ Slope $\geq 5\%$
Rangeland (R)	IR, DF, FMM, Urban	Not IR, not DF, not FMM, and not Urban

Euclidean Distance Method was used in performing segmentation using Euclidean distance for all band values for each pixel. The threshold distance of edge detection for best boundary delineation was set at five through trial and error, and was particularly critical for edges between dry farming and range areas. In this step, spectrally and spatially related partitions were formed. Zonal statistics were calculated as the distribution of classes from the previous step within each polygon resulting from the segmentation, and organized in a table. In the labelling process, a zonal statistics table was constituted based on polygons from the image segmentation process and classified map. The zonal statistics table presents a statistical distribution within each segmented polygon. As each segment polygon might house more than one class, each polygon was labelled based on the majority class within it (Figure 6).

2.2.6. *NDVI stratification*

For the subclasses of LC rangeland (Low-, Medium-, and High-Density ranges) another approach was required. To address this, the Landsat TM image was clipped (Figure 7, Step 19) so as to show only the R entity as defined by the results of Step 18 (Figure 6). From the original 410 ground-truth locations, 349 were known to be ranges of varying land cover density. These classified ground-truth points were overlaid with NDVI maps,

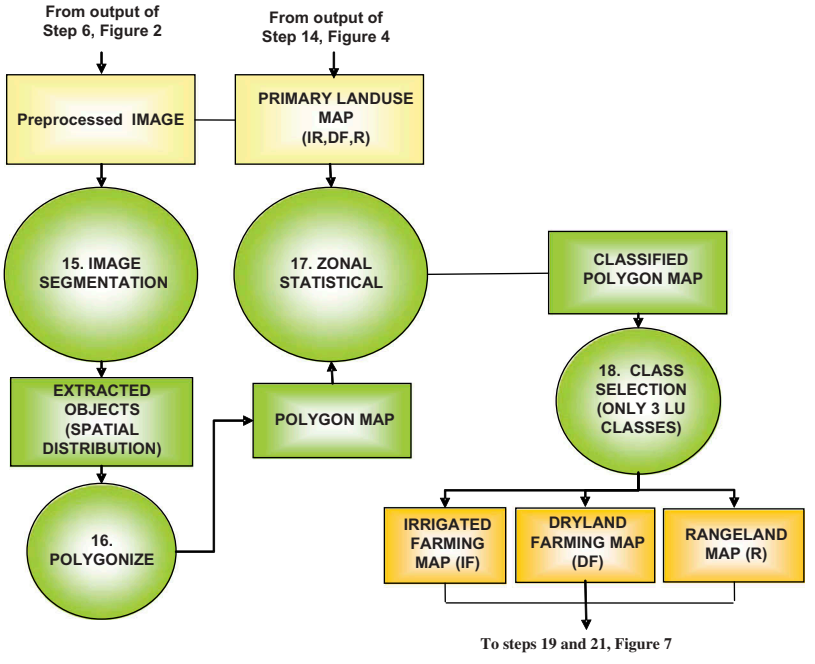

Figure 6. Enhancement of land-use (LU) classification via image segmentation and zonal statistics.

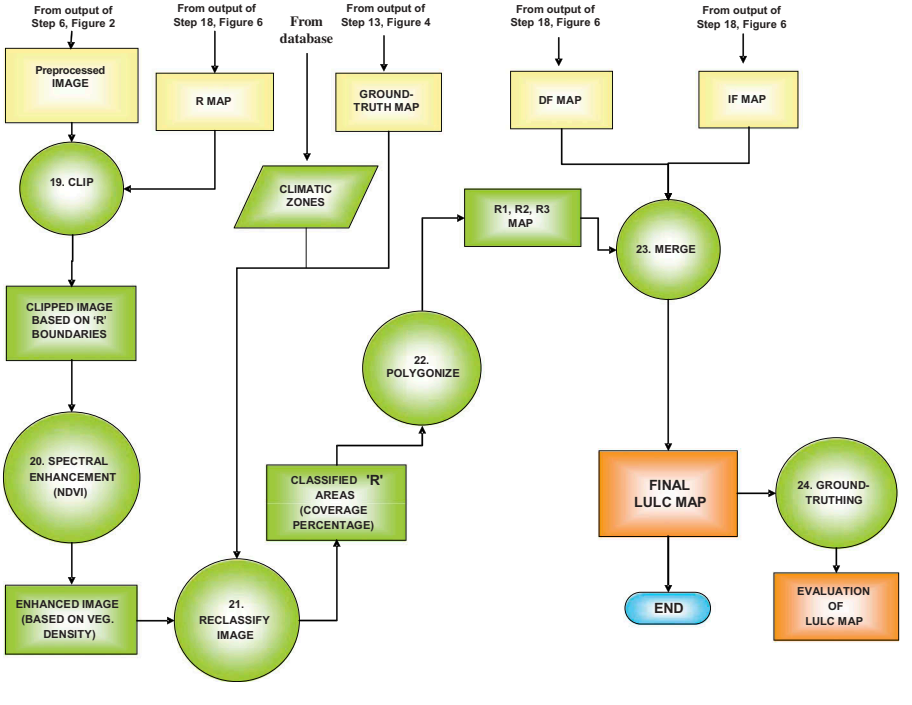

Figure 7. Enhancement of land-cover classification and creation of final LULC map.

Table 2. NDVI thresholds of each range class for each climate zone.

Climate zones	Range class	NDVI thresholds	
		Maximum	Minimum
Semi-Arid	Low-Density Rangeland	−0.109	−0.506
	Medium-Density Rangeland	0.308	−0.108
	High-Density Rangeland	0.508	0.309
Arid	Low-Density Rangeland	−0.147	−0.532
	Medium-Density Rangeland	0.284	−0.146
	High-Density Rangeland	0.472	0.285

and NDVI thresholds were calculated independently for each of two climate zones (Table 2). Using these thresholds, NDVI maps were sliced into three classes: Low-, Medium-, and High-Density ranges (Figure 7, Steps 20, 21, 22). The resulting layers were merged with Dryland Farming, Irrigated Farming, and Urban (Figure 7, Step 23) in order to generate a final LULC map.

2.3. *Map accuracy assessment*

To evaluate the accuracy of the LULC map, 410 reference sampling locations were chosen using a stratified random sampling procedure (Stehman 1999) so as to encompass the full variety of LULC classes across the whole study area. Class decisions were based on observing an area around the sampling location equal to 1–3 image pixels. All sites were visited and sampled by experienced agronomists with knowledge of the locality. Finally, an error matrix was generated to compare land-use and land-cover classifications resulting from the LULC map and the ground-truth classifications. The extent to which these two classifications agreed was measured by map producer's and user's accuracies (Congalton 1991), and by the kappa coefficient (Cohen 1960; Hudson and Ramm 1987). It should be noted that the field reference data were collected in the same month as images were acquired.

3. Results and discussion

The final LULC map is shown in Figure 8. Land-use and land-cover classes include Irrigated Farming, Dryland Farming, High-Density Rangeland (R1, cover > 30%, mostly between 30% and 50%), Medium-Density Rangeland (R2, 15 < cover ≤ 30%), Low-Density Rangeland (R3, cover ≥ 15%), Man-Made Forest, and Urban Area. The area and relative coverage of LULC classes in the study area (Figure 9) shows Medium-Density Rangeland to cover 109,078 ha or 53.5% of the whole study area, Low-Density Rangeland (59,682 ha, 29.3%.), High-Density Rangeland (22,791 ha, 11.2%), Irrigated Farming (7663 ha, 3.7%), and Dryland Farming (4009 ha, 2%).

The overall accuracy and kappa coefficient achieved were 88.3% and 0.83, respectively (Table 2). Producer's accuracy, a measure of how correct the classification is, ranged from a low of 65% in the case of Man-Made Forest to a high of 93.7% in the case of Irrigated Farming (Table 3). User's accuracy is a measure of the reliability of the map for each class, and ranged from a low of 60% in the case of Man-Made Forest to a high of 93.4% for Medium-Density Rangeland. Both producer's and user's accuracy were lowest for Man-Made Forest, which might be attributable to the class's small population

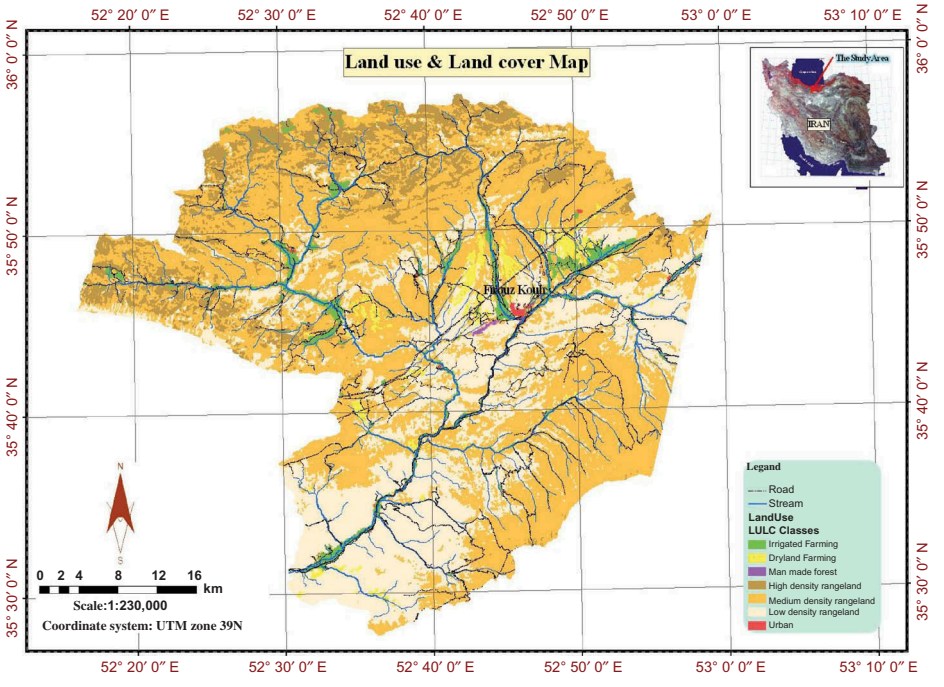

Figure 8. Final LULC map.

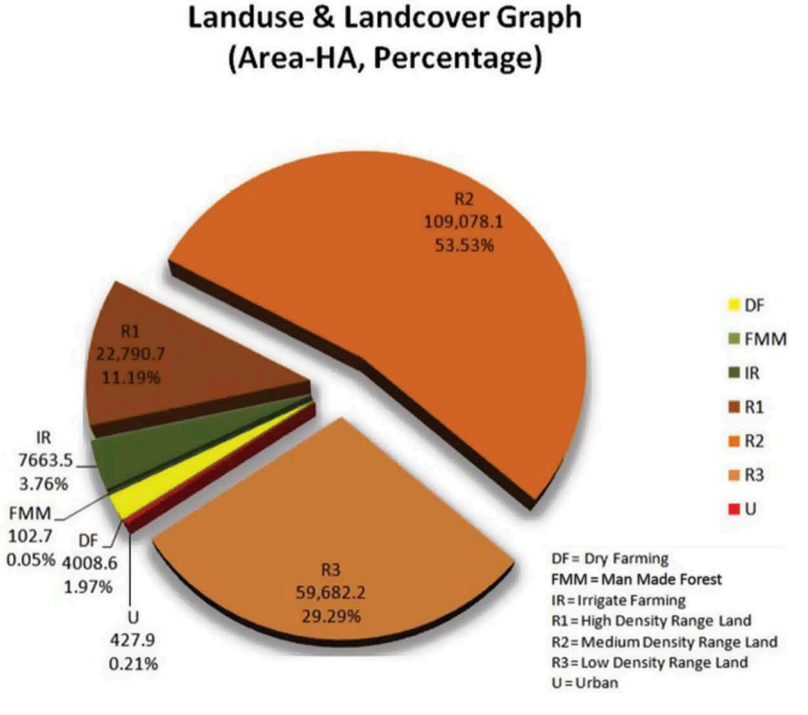

Figure 9. Area and percentage coverage of LULC classes for the study area.

Table 3. Accuracy assessment of land-use/land-cover classification (LULC) map.

Class		Reference total	Classified total	Number correct	Producer's accuracy (%)	User's accuracy (%)
IR	Irrigated Farming	32	37	30	93.75	81.08
DF	Dryland Farming	25	26	22	88.00	84.62
FMM	Man-Made Forest	4	5	3	75.00	60.00
R1	High-Density Rangeland	44	47	40	90.91	85.11
R2	Medium-Density Rangeland	193	183	171	88.60	93.44
R3	Low-Density Rangeland	112	112	96	85.71	85.71
Total		410	410	362		
Overall classification accuracy = 88.29%						
Kappa = 0.831						

size; indeed, Man-Made Forest covers less than 0.1% of the total study area. It should be noted that sparse trees including a few juniper species (5–25 trees per hectare) cover small parts of the study area, particularly steep, stony mountainsides. However, separation of this area into individual classes was not possible in this study. Thus, further work needs to be done in the future in regard to classification aspects of the LULC map.

All classes were well defined and differentiated, except the Forest class. This was particularly the case for Dryland Forest (PA = 88%), with its small area and diverse agricultural activities (e.g. varying planting and harvest dates, different locations and situations) presenting varying reflectance information on satellite images. The main land-use classes such as Irrigated Farming, Dryland Farming, Rangeland, and Man-Made Forest were differentiated through the step-by-step process of (i) image preprocessing; (ii) selection of training and reference sampling locations; (iii) use of the ICA method to decompose multi-spectral TM bands into features; (iv) land-use type classification based on slope and ICA method-derived features; (v) classified land-use map enhancement by image segmentation and zonal statistics; and (vi) enhancement of discrimination within the rangeland land-cover classification drawing on NDVI and climatic zones. Successful mapping, namely the delineation of what was otherwise overlapping information, was found to require going beyond the mere analysis of reflectance information, and incorporating climatic and topographic conditions.

Comparison of maps prepared by the Iranian Soil Conservation and Watershed Management Research Institute (SCWMRI, Table 4) and our LULC map developed in the present study (Table 2) shows the former to have major issues in differentiating among classes, particularly in defining areas of Dryland Farming, which results in mixing up of this class with Irrigated Farming or with Rangeland classes. Figures 10(*a*)–(*d*) show four areas of the watershed where our LULC map's land-use categories are colour-coded and labelled red, while the SCWMRI map's land-use categories are delimited by black lines and labelled black. In Figure 10(*a*) the SCWMRI map shows only two polygons (i.e. R2 and IR + DF) compared with five zones (R1, R2, R3, IR, and DF) for the new model. In general, the SCWMRI maps were able to identify Irrigated Farming better than the other land-use classes (Figure 10(*b*)). However, these maps were not able to distinguish between Dryland and Irrigated Farming separately, as shown in Figure 10(*a*). It may be seen from Figures 10(*a*), (*c*), and (*d*) that the polygon boundaries of Dryland Farming and

Table 4. Accuracy assessment of land-use and land-cover classification maps prepared by the Iranian Soil Conservation and Watershed Management Research Institute (SCWMRI).

Class		Reference total	Classified total	Number correct	Producer's accuracy (%)	User's accuracy (%)
Mixed (IR + DF)*	Irrigated Farming + Dry Farming	57	65	31	54.38	47.69
R1	High-Density Rangeland	44	62	30	61.18	48.39
R2	Medium-Density Rangeland	193	210	117	60.62	55.71
R3	Low-Density Rangeland	112	69	52	46.42	75.36
		406	406	230		
		Overall Classification Accuracy		56.65%		

Note: * SCWMRI maps were not able to distinguish individually between DF and IR.

Rangeland areas (R2 and R3) of SCWMRI maps exhibit significant overlap and have the least accurate results. This is likely because, in the case of Dryland Farming, there are diverse agricultural activities that result in diverse reflectance information in the satellite images. In turn, for some areas this makes Dryland Farming appear like R2 and R3 and renders differentiation difficult. On the other hand, decomposition of multi-spectral TM bands into features via the ICA method and using a number of ancillary layers (e.g. landform and climatic zone maps) helps address these issues. Field visits confirmed that polygon boundaries of the main land uses of the SCWMRI maps showed significant overlap, especially between Dryland Farming and Rangeland. It was found that all classes and polygon boundaries on the LULC map created in this study closely matched the situation in the field.

4. Conclusions and recommendations

Accurate land-use-land-cover classification (LULC) maps are central to watershed planning and management efforts, allowing for the development of sustainable land-use and resource allocation guidelines. However, these guidelines are only as good as the accuracy of the LULC maps. In Iran and many other developing countries around the world, currently available maps are fraught with limitations in regard to accuracy and discriminatory ability with regard to land use. While multi-spectral satellite imaging could address these issues, methods to extract the images and other geographic information's full potential need to be developed. To generate and validate a new approach to developing LULC maps (in this case for northeastern Iran's 2037.5 km^2 Hable-Roud watershed), a step-by-step process was developed and implemented, consisting of image preprocessing, extraction of training and reference sampling locations, decomposition of multi-spectral TM bands into features by ICA methods, classification using these features and slope maps, enhancement of land-use classes through image segmentation and zonal statistics, then through consideration of NDVI and climatic zones, followed by ground truthing.

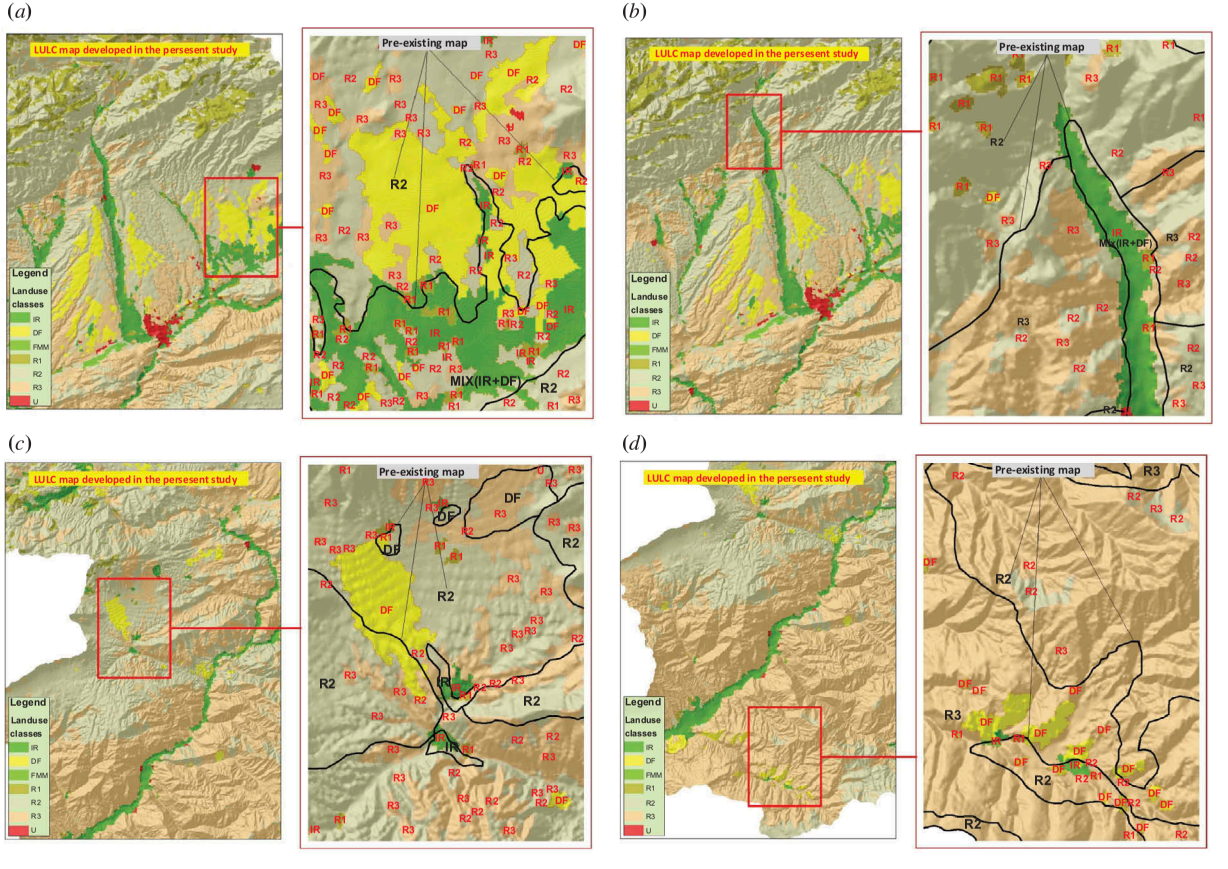

Figure 10. Comparison of LULC classes between the map developed in the present study (colour-coded and labelled red) and the pre-existing map (delineation with black lines and labelled black) in the study area.

While current maps only distinguished R1, R2, R3, and mixed Irrigated and Dryland Farming and must, at times, combine categories, the approach developed in this study was capable of greater discrimination, identifying and deliminating five different LU types: dryland farming, irrigated farmland, and low-, medium-, and high-vegetation density rangelands. The new maps' ground truthing-based overall accuracies and kappa coefficients were 88.3% and 0.83, respectively (as shown in Figures 10(*a*)–(*d*), the current maps have the least accurate results). The new maps' producer's and user's accuracies ranged from a low of 65% and 60%, respectively, for the least extensive land-use type (forest) to highs of 93.7% and 93.4% in the case of irrigated farmland. The new (vs. present) maps' greater discrimination and accuracy are apparent in Figure 10, where the new maps discriminated land uses far better than the old map. Developing the improved LULC map required going beyond the mere analysis of reflectance information, to incorporating climatic and topographic data through a step-by-step approach.

Acknowledgement

We are grateful for the constructive and valuable comments and suggestions given by Professor Mark Danson and an anonymous reviewer of our paper.

Funding

This research was partially funded by Natural Sciences and Engineering Research Council of Canada (NSERC) Discovery Grant, and a Canada Foundation for Innovation (CFI) grant held by Jan Adamowski.

References

Blaschke, T. 2010. "Object Based Image Analysis for Remote Sensing." *ISPRS Journal of Photogrammetry and Remote Sensing* 65 (1): 2–16. doi:10.1016/j.isprsjprs.2009.06.004.

Blaschke, T., C. Burnett, and A. Pekkarinen. 2004. "New Contextual Approaches Using Image Segmentation for Object-Based Classification." In *Remote Sensing Image Analysis: Including the Spatial Domain*, edited by F. De Meer and S. M. De Jong, 211–236. Dordrecht: Kluver Academic Publishers.

Blaschke, T., S. Lang, and G. J. Hay. 2008. *Object Based Image Analysis*, 817 pp. Heidelberg: Springer.

Chen, M., Y. Fu, D. Li, and Q. Qin. 2008. "Image Fusion Based on Extensions of Independent Component Analysis." In *International Society for Photogrammetry and Remote Sensing Archives* XXXVII, *Proceedings of the Conference XXIst ISPRS Congress, Technical Commission VII*, edited by C. Jun, J. Jie, and J. van Genderen, Beijing, July 3–11, 106–113. Part B7. http://www.isprs.org/proceedings/XXXVII/congress/tc7.aspx

Chen, Y., P. Shi, T. Fung, J. Wang, and X. Li. 2007. "Object-Oriented Classification for Urban Land Cover Mapping with ASTER Imagery." *International Journal of Remote Sensing* 28 (20): 4645–4651. doi:10.1080/01431160500444731.

Chitroub, S., and S. AlSultan. 2008. *Remote Sensing and Spatial Information Sciences* XXXVII. Part B7: 993–998.

Cihlar, J. 2000. "Land Cover Mapping of Large Areas from Satellites: Status and Research Priorities." *International Journal of Remote Sensing* 21 (6–7): 1093–1114. doi:10.1080/014311600210092.

Cohen, J. 1960. "A Coefficient of Agreement for Nominal Scales." *Educational & Psychological Measurement* 20: 36–46.

Colby, J. D. 1991. "Topographic Normalization in Rugged Terrain." *Photogrammetric Engineering & Remote Sensing* 57 (5): 531–537.

Comon, P. 1994. "Independent Component Analysis, a New Concept?" *Signal Processing* 36: 287–314. doi:10.1016/0165-1684(94)90029-9.

Congalton, R. G. 1991. "A Review of Assessing the Accuracy of Classifications of Remotely Sensed Data." *Remote Sensing of Environment* 37 (1): 35–46. doi:10.1016/0034-4257(91)90048-B.

Du, Q., I. Kopriva, and H. Szu. 2006. "Independent-Component Analysis for Hyperspectral Remote Sensing Imagery Classification." *Optical Engineering* 45 (1): 017008, 1–13.

Gamanya, R., P. de Maeyer, and M. de Dapper. 2009. "Object-Oriented Change Detection for the City of Harare, Zimbabwe." *Expert Systems with Applications* 36 (1): 571–588. doi:10.1016/j.eswa.2007.09.067.

Guerschman, J. P., J. M. Paruelo, C. Di Bella, M. C. Giallorenzi, and F. Pacin. 2003. "Land Cover Classification in the Argentine Pampas Using Multi-Temporal Landsat TM Data. Int." *International Journal of Remote Sensing* 24 (17): 3381–3402. doi:10.1080/0143116021000021288.

Houborg, R., and E. Boegh. 2008. "Mapping Leaf Chlorophyll and Leaf Area Index Using Inverse and Forward Canopy Reflectance Modeling and SPOT Reflectance Data." *Remote Sensing of Environment* 112 (1): 186–202. doi:10.1016/j.rse.2007.04.012.

Hudson, W. D., and C. W. Ramm. 1987. "Correct Formulation of the Kappa Coefficient of Agreement (In Remote Sensing)." *Photogrammetric Engineering & Remote Sensing* 53 (4): 421–422.

Im, J., J. R. Jensen, and J. A. Tullis. 2008. "Object-Based Change Detection Using Correlation Image Analysis and Image Segmentation." *International Journal of Remote Sensing* 29 (2): 399–423. doi:10.1080/01431160601075582.

Koohafkan, P., and B. A. Stewart. 2008. *Water and Cereals in Drylands*, 120 pp. London: Routledge.

Lackner, M., and T. M. Conway. 2008. "Determining Land-Use Information from Land Cover through an Object-Oriented Classification of IKONOS Imagery." *Canadian Journal of Remote Sensing* 34 (2): 77–92. doi:10.5589/m08-016.

Lobo, A. 1997. "Image Segmentation and Discriminant Analysis for the Identification of Land Cover Units in Ecology." *IEEE Transactions on Geoscience and Remote Sensing* 35 (5): 1136–1145. doi:10.1109/36.628781.

Martinuzzi, S., W. A. Gould, and O. M. Ramos González. 2007. "Land Development, Land Use, and Urban Sprawl in Puerto Rico Integrating Remote Sensing and Population Census Data." *Landscape and Urban Planning* 79: 288–297. doi:10.1016/j.landurbplan.2006.02.014.

Mousavi, S.-F. 2005. "Agricultural Drought Management in Iran." In *Committee on US–Iranian Workshop on Water Conservation and Recycling. Water Conservation, Reuse and Recycling*, 106–113. Washington, DC: National Academies Press. http://www.nap.edu/openbook.php?record_id=11241&page=106

Naik, G. R., and D. K. Kumar. 2011. "An Overview of Independent Component Analysis and Its Applications." *Informatica* 35: 63–81.

Ozdogan, M. 2010. "The Spatial Distribution of Crop Types from MODIS Data: Temporal Unmixing Using Independent Component Analysis." *Remote Sensing of Environment* 114: 1190–1204. doi:10.1016/j.rse.2010.01.006.

Renschler, C. S., and J. Harbor. 2002. "Soil Erosion Assessment Tools from Point to Regional Scales - the Role of Geomorphologists in Land Management Research and Implementation." *Geomorphology* 47: 189–209. doi:10.1016/S0169-555X(02)00082-X.

Royan Consulting Engineering. 2008. *The Study on Flood and Soil Erosion in the Hablehroud Watershed*. [In Farsi.] Tehran: Iranian Forest, Range and Watershed Management Organization, 245 pp.

Ruefenacht, B., D. Vanderzanden, M. Morrison, and M. Golden. 2002. "New Technique for Segmenting Images." An Image Segmentation Algorithm Developed by the USDA Forest Service, Remote Sensing Application Center. http://www.fs.fed.us/

Saadat, H., J. Adamowski, R. Bonnell, F. Sharifi, M. Namdar, and S. Ale-Ebrahim. 2011. "Land Use and Land Cover Classification over a Large Area in Iran Based on Single Date Analysis of Satellite Imagery." *ISPRS Journal of Photogrammetry and Remote Sensing* 66 (5): 608–619. doi:10.1016/j.isprsjprs.2011.04.001.

Saadat, H., R. Bonnell, F. Sharifi, G. Mehuys, M. Namdar, and S. Ale-Ebrahim. 2008. "Landform Classification from a Digital Elevation Model and Satellite Imagery." *Geomorphology* 100 (3–4): 453–464. doi:10.1016/j.geomorph.2008.01.011.

Saadat, H., and M. Namdar. 2012. *Technical Report on Hablehroud Watershed*, 105 pp. [In Farsi.] Tehran: Iranian Soil Conservation and Watershed Management Research Institute.

Shah, C. A. 2003. "Independent Component an Analysis Mixture Model (ICAMM) Algorithm for Unsupervised Classification of Multi/Hyper Spectral Imagery" Master's thesis., Syracuse, NY: Syracuse University, 188 pp.

Smith, J. A., T. L. Lin, and K. J. And Ranson. 1980. "The Lambertian Assumption and Landsat Data." *Photogrammetric Engineering & Remote Sensing* 46 (9): 1183–1189.

Stehman, S. V. 1999. "Basic Probability Sampling Designs for Thematic Map Accuracy Assessment." *International Journal of Remote Sensing* 20 (12): 2423–2441. doi:10.1080/014311699212100.

Thenkabail, P. S., E. A. Enclona, M. S. Ashton, C. Legg, and M. J. De Dieu. 2004. "Hyperion, IKONOS, ALI, and ETM+ Sensors in the Study of African Rainforests." *Remote Sensing of Environment* 90 (1): 23–43. doi:10.1016/j.rse.2003.11.018.

Tian, Q., Z. Luo, J. M. Chen, M. Chen, and F. Hui. 2007. "Retrieving Leaf Area Index for Coniferous Forest in Xingguo County, China with Landsat ETM+ Images." *Journal of Environmental Management* 85 (3): 624–627. doi:10.1016/j.jenvman.2006.05.021.

Woodcock, C., and V. J. Harward. 1992. "Nested-Hierarchical Scene Models and Image Segmentation." *International Journal of Remote Sensing* 13 (16): 3167–3187. doi:10.1080/01431169208904109.